

# A NUMERICAL METHOD FOR INTERFACE RECONSTRUCTION OF TRIPLE POINTS WITHIN A VOLUME TRACKING ALGORITHM

A. CABOUSSAT, M. M. FRANCOIS, R. GLOWINSKI, D. B. KOTHE, AND J. M. SICILIAN

ABSTRACT. A numerical method for the reconstruction of interfaces in finite volume schemes for multiphase flows is presented. The computation of the triple-point at the intersection of three materials in two dimensions of space is addressed. The determination of the normal vectors between pairs of materials is obtained with a finite element approximation. A numerical method for the localization of a triple-point is described as the minimum of a constrained minimization problem inside an interfacial cell of the discretization. For given volume fractions of materials in the cell, an interior-point/Newton method is used for the reconstruction of the local geometry and the localization of the triple-point. Initialization of the Newton method is performed with a derivative-free algorithm. Numerical results are presented for static and pure advection cases to illustrate the efficiency and robustness of the algorithm.

## 1. INTRODUCTION

Free surface flows appear in many fields of science and engineering, such as mold filling [10, 22], welding [7] or combustion and atomization [19].

In volume tracking finite volume based methods, see *e.g.* [29], the geometrical reconstruction of the interfaces between the various materials is a crucial issue in order to estimate accurately the propagation fronts. In volume-of-fluid methods, the description of the position of each material relies on the characteristic function of the domain filled with each material [20]. For both incompressible or compressible flows, the equations modeling the flow in each material are coupled with the advection equations governing the behavior of the volume fractions of materials [18]. In order to reconstruct a sharp approximation of the interfaces, a geometrical reconstruction locally in each interface cell of the discretization is needed to reduce the numerical diffusion and blurring of the propagation fronts induced by most algorithms. Several methods can be found in the literature for the reconstruction of an interface in two-phases flows, the most popular ones being the SLIC (*Simple line interface*

---

*Date:* May 12, 2008.

*Key words and phrases.* Interface reconstruction, Triple point configuration, Free Surface, Constrained Optimization, Multi-phase flows.

Corresponding author. Partially supported by University of Houston start-up funds.

Supported by Los Alamos National Laboratory. Operated by Los Alamos National Security, LLC, for the National Nuclear Security Administration of the U.S. Department of Energy under contract DE-AC52-06NA25396.

Partially supported by the National Science Foundation NSF-DMS 0412267.

Supported by Los Alamos National Laboratory. Operated by Los Alamos National Security, LLC, for the National Nuclear Security Administration of the U.S. Department of Energy under contract DE-AC52-06NA25396.

*calculation*) [9, 24, 26] or the PLIC (*Piecewise linear interface calculation*) [29, 30, 37, 32] procedures, the parabolic reconstruction of interfaces [28] or markers methods [2, 3]. In the SLIC method, the interface is reconstructed by determining the local normal vector to the interface and constructing a linear interface between two media that matches the volume fractions of materials in the cell, via a bisection method for instance [12, 29].

The two-dimensional case is discussed in this article. When three phases are adjacent in one cell, they can be arranged in layers or in a *triple-point configuration* where one point is located at the intersection of the three interface planes between pairs of materials [1, 14, 15, 31]. At equilibrium, the position of a triple-point and the orientation of the interfaces between pairs of materials can be determined by giving the *contact angles* between the interfaces, based on physical models or experimental data [17, 34]. However, in non-stationary cases, when the equilibrium between the different phases is not reached, the position of the triple-point and the orientation of the interfaces have to be reconstructed without relying on equilibrium angles. The reconstruction can rely on the approximation of normal vectors [1, 8] or be based on power diagrams [5, 31].

The approach presented here is an extension of the PLIC algorithm. The computation of a triple-point configuration requires i) the determination of the normal vectors of the interfaces between pairs of materials and ii) the localization of the triple-point in order to match the volume fractions of materials in the cell given by the finite volume method and the geometric volumes delimited by the triple-point and the three interfaces. The determination of the normal vectors is based on a finite element approach [6, 23]. For given normal vectors, the localization of the triple-point is based on a constrained minimization problem, solved with an interior-point method [25], coupled with a Newton iteration [36] and pattern-search techniques [13]. The procedure is based on the minimization of the difference between normalized computed volumes and volume fractions produced by the finite volume scheme, provided that the triple-point remains in the cell. As an extension of the PLIC algorithm, the proposed approach reconstruct linear interfaces and is therefore first order accurate.

The structure of this article is the following. In Section 2, the model for the flow and the volume fractions of materials is briefly presented. In Section 3, the computation of the normal vectors is presented and in Section 4, the problem of the localization of the triple-point is detailed. Finally, numerical results are presented in Section 5, in particular for the reconstruction of *T-shape* and *Y-shape* configurations.

## 2. GOVERNING EQUATIONS

The physical model considered is briefly described here; a complete description can be found in [12]. Let  $\Omega \subset \mathbb{R}^2$  be a bounded domain and  $\Gamma = \partial\Omega$  be its boundary. Let  $T > 0$  be a finite time and let  $M$  be the total number of materials/phases existing in the system.

The volume fractions describe the positions of the different materials. They are denoted by  $f_k$ ,  $k = 1, \dots, M$ , each of them being the characteristic function of the domain where the material  $k$  is present. Therefore  $f_k$  is equal to one in the phase  $k$ , zero outside and jumps across the interface.

Let  $\rho_k$  and  $\mu_k$ ,  $k = 1, \dots, M$  be the constant density and viscosity of the fluid in the phase  $k$ , respectively and  $\rho$  and  $\mu$  the piecewise constant functions defined respectively by  $\rho_k$  and  $\mu_k$  in the phase  $k$ .

The velocity and pressure of the fluid are denoted by  $\mathbf{u}$  and  $p$  respectively. For Newtonian fluids, the equations of conservation of mass and momentum in the space-time domain  $\Omega \times (0, T)$  are:

$$\begin{aligned} \frac{\partial \rho}{\partial t} + \nabla \cdot (\rho \mathbf{u}) &= 0, \\ \frac{\partial (\rho \mathbf{u})}{\partial t} + \nabla \cdot (\rho \mathbf{u} \mathbf{u}) &= -\nabla p + \nabla \cdot (\mu (\nabla \mathbf{u} + \nabla \mathbf{u}^T)) + \mathbf{f}, \end{aligned}$$

where  $\mathbf{f}$  denotes the surface and body forces applied onto the fluid. In the particular case of incompressible immiscible fluids of different constant densities, the conservation of mass gives  $\nabla \cdot \mathbf{u} = 0$  in each phase [18]. Appropriate initial and boundary conditions are prescribed. In particular, on the free boundaries (interfaces between materials), the normal velocity is continuous and surface tension effects are taken into account, so that the equilibrium force balance is given by  $[-p\mathbf{n} + \mu(\nabla \mathbf{u} + \nabla \mathbf{u}^T)\mathbf{n}] = \sigma \kappa \mathbf{n}$ , where  $\mathbf{n}$  denotes the normal vector to the interface between the two phases,  $\sigma$  is the constant surface tension coefficient (depending on the two adjacent phases),  $\kappa$  is the curvature of the interface, and  $[\cdot]$  denotes the jump of a quantity across the interface.

The conservation of mass, the immiscible fluid property, and the constant density  $\rho_k$  leads to

$$\frac{\partial f_k}{\partial t} + \mathbf{u} \cdot \nabla f_k = -f_k \nabla \cdot \mathbf{u} = 0, \quad \text{in } \Omega \times (0, T), \quad k = 1, \dots, M. \quad (1)$$

This relation is an evolution equation for the location of each phase. The numerical solution to (1) is given by a finite volume scheme. Computation of the fluxes at the boundaries of a cell are determined by the geometric reconstruction of the local interfaces inside each interface cell. Details of the numerical scheme can be found in [18]. In the following we focus on the geometrical reconstruction of the interfaces for triple-point configurations and the consequences on the accuracy and consistency of computation of fluxes, especially for coarse meshes.

### 3. COMPUTATION OF NORMAL VECTORS AND ORIENTATION OF INTERFACES

Let  $Q_h$  be a quadrangulation of  $\Omega$ ,  $h$  the mesh size, and  $Q \in Q_h$  a generic cell of the quadrangulation (quadrilateral). Let  $V_Q$  denote the surface of the cell  $Q$ . Let  $N_c$  be the number of cells in  $Q_h$ . For the characteristic function  $f$  of any material domain, the finite volume scheme presented in [18] provides a piecewise constant approximation of  $f$  in  $Q_h$ , denoted by  $f_{0,h}$ , with values located at the center of the cells.

In the case of two materials in the same cell  $Q$ , planar interfaces are geometrically constructed to determine the boundary between the two materials in each mixed cell  $Q$ , by using the PLIC algorithm (*piecewise linear interface calculation*) [29]. The case of three materials in the same cell is addressed in the sequel.

For the characteristic function  $f$  of the material domain, the approximation of the normal vector  $\mathbf{n}$  oriented outside the material domain is computed here in a finite element framework. Let us denote by  $\mathcal{T}_h$  a nested finite element mesh

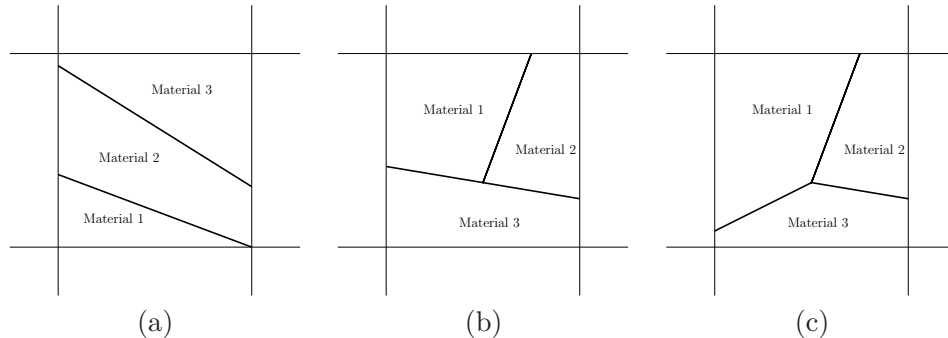


FIGURE 1. Topology situations for the local reconstruction of the interfaces inside the cell; (a) layers configuration, (b) triple-point configuration in T-shape configuration, (c) triple-point configuration in Y-shape configuration

constructed by dividing one quadrilateral  $Q \in Q_h$  into eight triangles such that each triangle has one vertex in the center of the cell, one in the center of a face of the cell and the remaining vertex is superimposed with one vertex of the cell. Let  $K$  denote a generic triangle of  $\mathcal{T}_h$ . The number of vertices in  $\mathcal{T}_h$  is denoted by  $N_n$ , the piecewise linear finite element basis functions based on  $\mathcal{T}_h$  being denoted by  $\varphi_j$ ,  $j = 1, \dots, N_n$ . The piecewise linear approximation of any volume fraction  $f$  on  $\mathcal{T}_h$  is noted  $f_{1,h}$  and given by the  $L^2$ -projection of  $f_{0,h}$  defined by

$$\int_{\Omega} f_{1,h} \varphi_j dx = \int_{\Omega} f_{0,h} \varphi_j dx, \forall j = 1, \dots, N_n.$$

The projection allows one to obtain a piecewise linear approximation  $f_{1,h}$  on the finite element mesh. The approximation  $f_{1,h}$  is differentiated to obtain a piecewise constant value  $\nabla f_{1,h}$  on each  $K \in \mathcal{T}_h$ , that is normalized locally to give the normal vector  $\mathbf{n}_{1,h}$ . The value of the normal vector at the vertices of  $\mathcal{T}_h$  is denoted by  $\mathbf{n}_{0,h}$  and is given by the projection of the piecewise constant field  $\mathbf{n}_{1,h}$  on the vertices of the finite element mesh:

$$\int_{\Omega} \mathbf{n}_{0,h} \varphi_j dx = \int_{\Omega} \mathbf{n}_{1,h} \varphi_j dx, \forall j = 1, \dots, N_n.$$

The accuracy of the method has been discussed in [6]. The procedure is repeated for all three phases.

Figure 1 illustrates the possible configurations with three materials in a cell  $Q$ . The three materials can either be arranged in layers (Figure 1 (a)), or in a star-shaped configuration that splits the cell in three regions that are adjacent in one point called the *triple-point* (Figure 1 (b) and (c)). The general configuration (c) is referred to as the *Y-shape* configuration, while the case (b) when two interfaces of the star-shaped configuration are aligned (one contact angle is equal to  $\pi$ ) is referred to as the *T-shape* configuration.

The *onion skin* model [12, 37] allows one to reconstruct layers configurations (see Figure 1 (a)). The materials are arbitrarily ordered and the ordered volume fractions are denoted by  $f_{i_1}, f_{i_2}, f_{i_3}$ . The derivatives  $\nabla f_{i_1}, \nabla(f_{i_1} + f_{i_2})$  are successively computed to determine the orientation of the interfaces between the material  $i_1$

and  $i_2$  and  $i_2$  and  $i_3$  respectively. The ordering of the materials is set *a priori* and may lead to non-physical reconstructions. For instance, geometric reconstructed interfaces can cross each other.

The *T-shape* configuration shown in Figure 1 (b) can be treated with two successive applications of the PLIC algorithm as in [8]. In the following, a treatment of the general *Y-shape* triple-point configurations (Figure 1 (c)) is presented. Alternative reconstructions can be found for instance in [1, 8, 14, 15].

The algorithm to distinguish between these various configurations in a cell  $Q$  relies on the values of the volumes fractions of liquid  $f_{1,h}$  of the three materials in the cells in the neighborhood of  $Q$ . We assume there exist cells adjacent to  $Q$  that contain exact pairs of materials. That means, for each pair of material  $(i, j)$ , there exists a unique cell  $Q'$ , adjacent to  $Q$ , that contains material  $i$  and  $j$  only.

In the cell  $Q'$  that contains two materials  $i$  and  $j$ , the normal vector oriented towards the material  $j$ , is given before normalization by:

$$\mathbf{n}_{ij} = \frac{\nabla f_i}{|\nabla f_i|} - \frac{\nabla f_j}{|\nabla f_j|}. \quad (2)$$

Both vectors  $\frac{\nabla f_i}{|\nabla f_i|}$  and  $\frac{\nabla f_j}{|\nabla f_j|}$  are computed with finite element techniques as presented before. The minus sign is introduced to average two vectors oriented towards the material  $j$  and preserve symmetries, as illustrated by numerical results in Section 5. When the averaging is not considered, a bias may be introduced in the computation of the normal vectors by the arbitrary ordering of the three materials.

Once the normal vectors in cells with two materials are obtained, we consider one generic cell  $Q$  which contains three phases and denote by  $f_k > 0$ ,  $k = 1, 2, 3$ , the volume fractions of the three materials in this cell. Once the normal vector between materials  $i$  and  $j$  has been determined by (2) in the cell  $Q'$ , its value determines the normal vector between materials  $i$  and  $j$  in the original cell  $Q$ . This procedure is repeated for the successive pairs of materials. By convention, for the interface between materials 1 and 2 (resp. 2 and 3), the normal vector is oriented towards the material 2 (resp. 3). For the interface between materials 3 and 1, the normal vector is oriented towards the material 1.

#### 4. AN INTERIOR-POINT METHOD FOR THE LOCALIZATION OF THE TRIPLE POINT

**4.1. Minimization Algorithm.** An optimization method for the localization of the triple-point is presented. The mesh is not necessarily orthogonal along the  $Ox$  and  $Oy$  directions. For any pairs of materials  $i_1$  and  $i_2$ , the normal vectors to the interfaces between the materials  $i_1$  and  $i_2$  in a cell with three phases are computed with the procedure described in Section 3. The numerical method for the determination of the position of the triple-point is detailed here for a given set of three normal vectors.

Given the three normal vectors to the interfaces between pairs of materials, any point in the cell splits the cell into three regions, as illustrated in Figure 2. The volumes  $V_j$ ,  $j = 1, 2, 3$ , of these three regions can be computed and normalized by the volume  $V_Q$  of the cell  $Q$ , to be compared to the volume fractions  $f_j$ ,  $j = 1, 2, 3$ . A sequence of points in the cell is then computed in order to minimize the difference between  $V_j/V_Q$  and  $f_j$ , until a stationary solution is reached. The sequence of iterates is constrained in order to remain in the cell. This iterative procedure

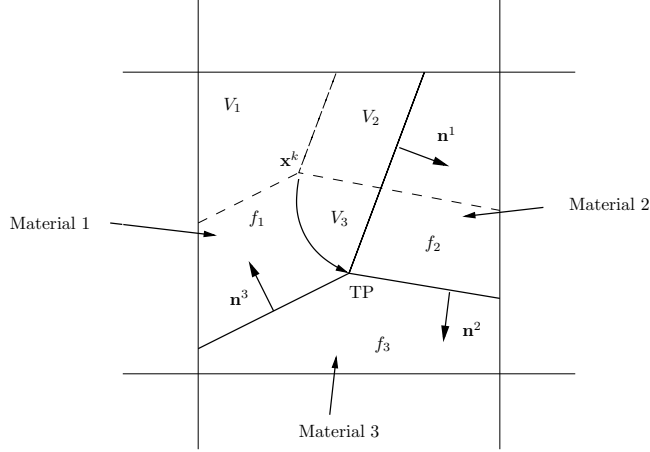


FIGURE 2. Triple-point interfaces: the situation inside one two-dimensional cell. The point  $\mathbf{x}^k$  splits the cells in three regions with volumes  $V_j$ . The point is updated in order for the volumes  $V_j/V_Q$  to match with  $f_j$ ,  $j = 1, 2, 3$ ,  $TP$  denotes the triple-point location.

requires the computation of the volumes delimited by the iterates of the triple-point in the cell and the computation of a descent direction to update the triple-point position.

The normal vectors between every pair of materials are denoted by  $\mathbf{n}^\alpha$ ,  $\alpha = 1, 2, 3$ . Let us denote by  $TP$  the triple-point and by  $\mathbf{x}^k$ ,  $k = 0, 1, 2, \dots$  the iterates generated by the method. Since  $\sum_{j=1}^3 f_j = \sum_{j=1}^3 \frac{V_j}{V_Q} = 1$ , the objective function  $g : \mathbb{R}^2 \rightarrow \mathbb{R}^2$  is given by:

$$g(x, y) = \begin{pmatrix} V_1(x, y)/V_Q \\ V_2(x, y)/V_Q \end{pmatrix} - \begin{pmatrix} f_1 \\ f_2 \end{pmatrix}. \quad (3)$$

The geometric volumes  $V_i(x, y)$ ,  $i = 1, 2$  are defined by  $\mathbf{x} = (x, y)$  and the intersections points of the lines that go through  $\mathbf{x}$ , with normal vectors  $\mathbf{n}^\alpha$ , with the faces of the cell. The point  $TP = (x, y)$  in the cell  $Q$  such that  $g(x, y) = 0$  is the triple-point. The problem of finding a root of (3) can be treated with a least squares-like method, under the constraints that the point  $TP$  remains in the cell  $Q$ . Let  $\mathbf{A} \in \mathbb{R}^{4 \times 2}$  and  $\mathbf{b} \in \mathbb{R}^4$  be the matrix and vector such that the equation  $\mathbf{A}\mathbf{x} = \mathbf{b}$  describes the equations of the four faces of  $Q$ . The condition  $\mathbf{x} \in Q$  is therefore equivalent to the inequalities  $\mathbf{A}\mathbf{x} \geq \mathbf{b}$ . The triple-point is expressed as the solution of the following constrained minimization problem:

$$\min_{\mathbf{x} \in \mathbb{R}^2} G(\mathbf{x}), \quad \text{s. t.} \quad \mathbf{A}\mathbf{x} \geq \mathbf{b}, \quad (4)$$

where  $G : \mathbb{R}^2 \rightarrow \mathbb{R}$  is a potential such that  $g(x, y) = \nabla G(x, y)$ . Slack variables  $z = \mathbf{A}\mathbf{x} - \mathbf{b} \in \mathbb{R}^4$  are introduced. The first order optimality conditions (Karush-Kuhn-Tucker conditions) relative to (4) therefore read

$$\begin{aligned} g(\mathbf{x}) - \mathbf{A}^T \mu &= 0 \\ \mathbf{A}\mathbf{x} - z - \mathbf{b} &= 0 \\ z \geq 0, \mu \geq 0, z\mu &= 0 \end{aligned}, \quad (5)$$

where  $\mu \in \mathbb{R}^4$  are the dual variables associated to the equality constraints  $\mathbf{A}\mathbf{x} - z - \mathbf{b} = 0$ , which are introduced in the Lagrangian function  $\mathcal{L}(\mathbf{x}, z, \mu) = G(\mathbf{x}) - \mu^T(\mathbf{A}\mathbf{x} - z - \mathbf{b})$ . The last equation in (5) corresponds to the strict complementarity conditions due to the inequalities  $z \geq 0$ . It corresponds to  $z_i \mu_i = 0$ ,  $i = 1, \dots, 4$ . The strict complementarity conditions are relaxed with an interior-point method [25]. A parameter  $\nu > 0$  is introduced so that they are replaced by the weaker formulation:

$$z > 0, \mu > 0, z\mu = \nu.$$

The inequality constraints are therefore removed. The sequence of estimates  $\mathbf{x}, \mu, z$  obtained for given  $\nu$  converges to the solution to (5) when the parameter  $\nu$  tends to zero [16]. The corresponding (unconstrained) nonlinear system of equations reads:

$$\begin{aligned} g(\mathbf{x}) - \mathbf{A}^T \mu &= 0 \\ \mathbf{A}\mathbf{x} - z - \mathbf{b} &= 0 \\ \mu - \frac{\nu}{z} &= 0 \end{aligned}. \quad (6)$$

The last equation is satisfied component by component, *i.e.*  $\mu_i - \nu/z_i = 0$ ,  $i = 1, \dots, 4$ . For given  $\nu$ , the nonlinear system (6) is solved with a Newton method. The displacements  $p_{\mathbf{x}} \in \mathbb{R}^2$ ,  $p_z \in \mathbb{R}^4$  and  $p_{\mu} \in \mathbb{R}^4$  for the variables  $\mathbf{x}^k$ ,  $z^k$ ,  $\mu^k$  at iterate  $k$  are the solutions to the KKT Newton system:

$$\begin{pmatrix} \nabla g(\mathbf{x}^k) & 0 & -\mathbf{A}^T \\ 0 & \text{diag}\left(\frac{\nu}{(z^k)^2}\right) & I \\ -\mathbf{A} & I & 0 \end{pmatrix} \begin{pmatrix} p_{\mathbf{x}} \\ p_z \\ p_{\mu} \end{pmatrix} = - \begin{pmatrix} g(\mathbf{x}^k) - \mathbf{A}^T \mu^k \\ \mu^k - \nu/z^k \\ \mathbf{b} - \mathbf{A}\mathbf{x}^k + z^k \end{pmatrix}, \quad (7)$$

and the variables  $\mathbf{x}^{k+1} = \mathbf{x}^k + p_{\mathbf{x}}$ ,  $z^{k+1} = z^k + p_z$  and  $\mu^{k+1} = \mu^k + p_{\mu}$  are updated, together with a step-length search if needed. Then  $\nu$  is reduced and a Newton step is repeated. The function  $g$  is piecewise continuously differentiable (PC<sup>1</sup>), since the derivatives are discontinuous when the iterate  $\mathbf{x}^k$  is such that one interface between two materials hits one corner of the cell (see Section 4.3). When the three normal vectors  $\mathbf{n}^\alpha$ ,  $\alpha = 1, 2, 3$  are nearly colinear, the KKT system (7) is ill-conditioned or the Newton iterates converge to a point on the boundary of the cell. This criterion is used to switch to the onion skin model [12, 37] for a layers configuration.

The implementation of the algorithm is as follows. An initial guess  $\mathbf{x}^0$  of the triple-point is obtained with a *pattern-search* derivative-free algorithm, see Section 4.2. Then for  $k \geq 0$ , (7) is solved to obtain a descent direction and the iterate  $\mathbf{x}^{k+1}$  is obtained. In order to solve (7), the function  $g$  and its derivatives  $\nabla g$  are computed analytically almost everywhere, as detailed in Section 4.3.

The minimization problem (4) does not necessarily admit a minimizer that satisfies  $g(\mathbf{x}) = 0$ . More precisely, if there exists  $\mathbf{x} \in Q$  such that  $g(\mathbf{x}) = 0$ , the interior-point/Newton algorithm converges to  $\mathbf{x}$  if the initial guess is in a neighborhood of the solution, while, if  $g(\mathbf{x}) \neq 0$ ,  $\forall \mathbf{x} \in Q$ , then  $\mu \neq 0$  and (6) gives  $z = 0$  when  $\nu \rightarrow 0$ , by strict complementarity. In that case, the algorithm converges to a

point  $\mathbf{x} \in \partial Q$  and switches to the onion-skin configuration. The Newton method applied to (6) converges quadratically in the neighborhood of the solution, even if  $g$  is piecewise continuously differentiable (see Section 4.3) [21, 35]. The local convergence of the Newton method is the reason of the addition of a pattern-search derivative-free algorithm for its initialization, which allows to conclude to the global convergence of the whole algorithm for any guess point in the cell.

**4.2. Initial Guess for the Newton Method.** The Newton approach can be coupled with a derivative-free pattern-search method [11, 13, 33] for a better initial guess of the Newton iterations and global convergence properties. The initial guess for the sequence generated by the Newton method is located at the center of the cell. An *alternated-direction search* is then applied locally to find a descent direction based only on the values of the objective function  $g$ . Let us denote by  $\mathbf{e}_j$  the directions along each coordinate axis and  $\Delta^k$  be a step length. When the mesh is orthogonal, the exploratory moves are defined with the following algorithm.

- (1) Given  $\mathbf{x}^k$ ,  $\Delta^k$  and  $\|g(\mathbf{x}^k)\|$ , set  $s_k = 0$  and  $\min = \|g(\mathbf{x}^k)\|$ .
- (2) For  $i = 1, 2, \dots$ 
  - a)  $s_k^i = s_k + \Delta^k \mathbf{e}_i$  and  $\mathbf{x}_i^k = \mathbf{x}^k + s_k^i$ . Compute  $\|g(\mathbf{x}_i^k)\|$ .
  - b) If  $\|g(\mathbf{x}_i^k)\| < \min$ , then  $\min = \|g(\mathbf{x}_i^k)\|$  and  $s_k = s_k^i$ . Otherwise
    - i)  $s_k^i = s_k^i - \Delta^k \mathbf{e}_i$  and  $\mathbf{x}_i^k = \mathbf{x}^k + s_k^i$ . Compute  $\|g(\mathbf{x}_i^k)\|$ .
    - ii) If  $\|g(\mathbf{x}_i^k)\| < \min$ , then  $\min = \|g(\mathbf{x}_i^k)\|$  and  $s_k = s_k^i$ .

When the mesh is not orthogonal, the directions  $\mathbf{e}_i$  are replaced by the average of the tangential vectors to two opposite faces.

**4.3. Computation of Volumes and Derivatives.** In the numerical resolution of (7), the evaluation of the function  $g$  and its derivatives  $\nabla g$  is required. The function  $g$  is expressed through the volumes  $V_1$  and  $V_2$  occupied by the materials 1 and 2 in the cell. The analytic expressions of the volumes and their derivatives are presented here, for arbitrary meshes (with cells that are not necessarily squares or rectangles). The  $k^{\text{th}}$  iterate  $\mathbf{x}^k = (x^k, y^k)$  and the normal vectors  $\mathbf{n}^\alpha = (\mathbf{n}_x^\alpha, \mathbf{n}_y^\alpha)^T$ ,  $\alpha = 1, 2, 3$  are assumed to be given. The intersection points  $\mathbf{x}_\alpha^k = (x_\alpha^k, y_\alpha^k)$ ,  $k = 1, 2, 3$  of the material interfaces with the faces of the cell are given by:

$$\begin{cases} x_\alpha^k = \frac{1}{\mathbf{n}^\alpha \cdot \mathbf{t}} (\mathbf{t}_x (\mathbf{n}^\alpha \cdot \mathbf{x}^k) + \mathbf{n}_y^\alpha \mathbf{F}) \\ y_\alpha^k = \frac{1}{\mathbf{n}^\alpha \cdot \mathbf{t}} (\mathbf{t}_y (\mathbf{n}^\alpha \cdot \mathbf{x}^k) - \mathbf{n}_x^\alpha \mathbf{F}) \end{cases}, \quad (8)$$

where  $\mathbf{t} = \mathbf{c}_1 - \mathbf{c}_2$  is the tangential vector to the face on which the intersection point  $\mathbf{x}_\alpha^k$  lies,  $\mathbf{c}_1, \mathbf{c}_2$  are the vertices of that face and  $\mathbf{F} := \mathbf{t}_y \mathbf{c}_{1,x} - \mathbf{t}_x \mathbf{c}_{1,y}$ . One can check that these points are the intersection points between the two lines  $\mathbf{n}_x^\alpha x + \mathbf{n}_y^\alpha y - (\mathbf{n}_x^\alpha x^k + \mathbf{n}_y^\alpha y^k) = 0$  (equation of the line going through  $\mathbf{x}^k$  and with given normal vector  $\mathbf{n}^\alpha$ ) and  $\mathbf{t}_y x - \mathbf{t}_x y - (\mathbf{t}_y \mathbf{c}_{1,x} - \mathbf{t}_x \mathbf{c}_{1,y}) = 0$  (equation of the face with given tangential vector  $\mathbf{t} = \mathbf{c}_1 - \mathbf{c}_2$ ).

The computation of the intersection point of the oriented interface with one face of the cell (together with the recognition of this face) is based on (8). For each interface (*i.e.* for each pair of materials) and for each face  $f = 1, \dots, 4$  of the cell, we do

- (i) Compute the intersection point of the interface with the face with (8).

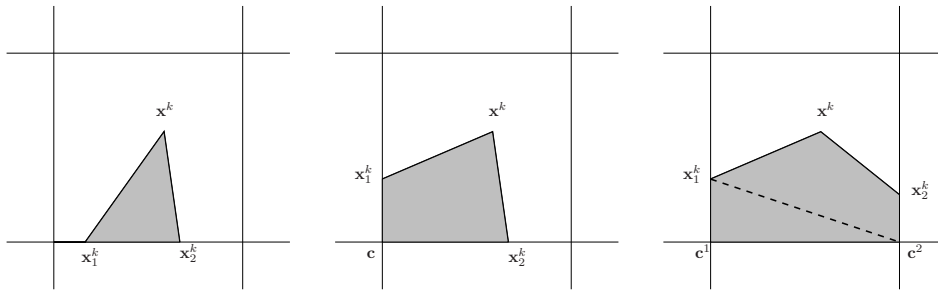


FIGURE 3. Computation of the volumes. Left : the volume is a triangle (both intersection points  $\mathbf{x}_1^k$  and  $\mathbf{x}_2^k$  are on the same face), middle: the volume is a quadrilateral (intersection points  $\mathbf{x}_1^k$  and  $\mathbf{x}_2^k$  are on adjacent faces), or right: the volume is a pentahedral (intersection points  $\mathbf{x}_1^k$  and  $\mathbf{x}_2^k$  are on opposite faces).

- (ii) Check that the intersection point is inside the segment  $[\mathbf{c}_1, \mathbf{c}_2]$ , *i.e.*  $(\mathbf{x}_\alpha^k - \mathbf{c}_1) \cdot (\mathbf{x}_\alpha^k - \mathbf{c}_2) < 0$ .

Once the intersection points are known, the computation of the partial volumes is achieved. Let  $\mathbf{a}, \mathbf{b}, \mathbf{c}, \mathbf{d}$  be four points of  $\mathbb{R}^2$ . For any oriented quadrilateral  $\mathbf{abcd}$  (with counter-clockwise orientation), the geometrical (positive) volume is given by

$$V(\mathbf{abcd}) = \frac{1}{2} (\mathbf{a} - \mathbf{c}) \times (\mathbf{b} - \mathbf{d}). \quad (9)$$

Relationship (9) also holds for a triangle when two vertices of the quadrilateral are superimposed. The truncated region of the cell by a given phase is determined by the iterate  $\mathbf{x}^k$ , two intersection points  $\mathbf{x}_\alpha^k$  and  $\mathbf{x}_\beta^k$ , and zero, one or two vertices of the cell. Figure 3 shows a sketch of the three possible configurations for the volumes. The truncated volumes are expressed by volumes of quadrilaterals (eventually degenerated into a triangle), or sum of such volumes as in Figure 3 (right) and their volumes is computed with (9) as the sum of one or several quadrilaterals.

If the normal vectors to the interfaces  $\mathbf{n}^\alpha$  and  $\mathbf{n}^\beta$  are given, the volumes of the regions occupied by the various materials are polynomial functions of degree two in terms of the coordinates  $(x, y)$  of  $\mathbf{x}^k$ . First consider the situation represented in Figure 3 (middle); let us denote by  $\mathbf{x}_1^k = (x_1^k, y_1^k)$  and  $\mathbf{x}_2^k = (x_2^k, y_2^k)$  the two intersections points of the interfaces with the faces of the cell, by  $\mathbf{x}^k \mathbf{x}_1^k \mathbf{c} \mathbf{x}_2^k$  the oriented volume/surface, where  $\mathbf{c}$  is the cell vertex enclosed between the two faces, and by  $\mathbf{t}^i = \mathbf{x}_i^k - \mathbf{c}$ ,  $i = 1, 2$  the tangent vector on each face of the cell. Relationship (8) implies

$$\begin{aligned}
V &= \frac{1}{2} (\mathbf{x}^k - \mathbf{c}) \times (\mathbf{x}_2^k - \mathbf{x}_1^k) \\
&= \frac{1}{2} \left\{ x^2 \left( \frac{\mathbf{t}_y^2 \mathbf{n}_x^2}{\mathbf{n}^2 \cdot \mathbf{t}^2} - \frac{\mathbf{t}_y^1 \mathbf{n}_x^1}{\mathbf{n}^1 \cdot \mathbf{t}^1} \right) + y^2 \left( \frac{\mathbf{t}_x^1 \mathbf{n}_y^1}{\mathbf{n}^1 \cdot \mathbf{t}^1} - \frac{\mathbf{t}_x^2 \mathbf{n}_y^2}{\mathbf{n}^2 \cdot \mathbf{t}^2} \right) \right. \\
&\quad + xy \left( \frac{1}{\mathbf{n}^1 \cdot \mathbf{t}^1} (\mathbf{t}_x^1 \mathbf{n}_x^1 - \mathbf{t}_y^1 \mathbf{n}_y^1) + \frac{1}{\mathbf{n}^2 \cdot \mathbf{t}^2} (\mathbf{t}_y^2 \mathbf{n}_y^2 - \mathbf{t}_x^2 \mathbf{n}_x^2) \right) \\
&\quad + x \left( \frac{1}{\mathbf{n}^1 \cdot \mathbf{t}^1} (\mathbf{n}_x^1 \mathbf{F}^1 - \mathbf{c}_y \mathbf{t}_x^1 \mathbf{n}_x^1) + \frac{1}{\mathbf{n}^2 \cdot \mathbf{t}^2} (-\mathbf{n}_x^2 \mathbf{F}^2 + \mathbf{c}_y \mathbf{t}_x^2 \mathbf{n}_x^2) \right) \\
&\quad + y \left( \frac{1}{\mathbf{n}^1 \cdot \mathbf{t}^1} (\mathbf{n}_y^1 \mathbf{F}^1 + \mathbf{c}_x \mathbf{t}_y^1 \mathbf{n}_y^1) + \frac{1}{\mathbf{n}^2 \cdot \mathbf{t}^2} (-\mathbf{n}_y^2 \mathbf{F}^2 - \mathbf{c}_x \mathbf{t}_y^2 \mathbf{n}_y^2) \right) \\
&\quad \left. + \text{constant} \right\}, \tag{10}
\end{aligned}$$

where  $\mathbf{F}^i = \mathbf{t}_y^i \mathbf{c}_x^i - \mathbf{t}_x^i \mathbf{c}_y^i$ ,  $i = 1, 2$ .

Similar analytical expressions are obtained for the volume in Figure 3 (right): when the volume is an oriented pentahedral  $\mathbf{x}^k \mathbf{x}_1^k \mathbf{c}^1 \mathbf{x}_2^k$ , it is decomposed into a quadrilateral  $\mathbf{x}^k \mathbf{x}_1^k \mathbf{c}^2 \mathbf{x}_2^k$  and a triangle  $\mathbf{x}_1^k \mathbf{c}^1 \mathbf{c}^2$ . Relationship (10) is used for the quadrilateral. Concerning the triangle  $\mathbf{x}_1^k \mathbf{c}^1 \mathbf{c}^2$ , the mid-point  $\mathbf{m} = \frac{1}{2}(\mathbf{c}^1 + \mathbf{c}^2)$  is introduced. Relationships (8) and (9) lead to

$$V = \frac{1}{2} \{ (\mathbf{c}_y^1 - \mathbf{c}_y^2) x_2^k - (\mathbf{c}_x^1 - \mathbf{c}_x^2) y_2^k + \mathbf{m}_y (\mathbf{c}_x^1 - \mathbf{c}_x^2) - \mathbf{m}_x (\mathbf{c}_y^1 - \mathbf{c}_y^2) \}. \tag{11}$$

One can check that the volume (11) is independent of the choice of the auxiliary point  $\mathbf{m}$  in the segment  $[\mathbf{c}_1, \mathbf{c}_2]$ . The last case is the situation represented in Figure 3 (left). The surface  $\mathbf{x}^k \mathbf{x}_1^k \mathbf{x}_2^k$  is expressed as the quadrilateral  $\mathbf{x}^k \mathbf{x}_1^k \mathbf{x}_1^k \mathbf{x}_2^k$ , so that (9) leads to:

$$\begin{aligned}
V &= \frac{1}{2} \left\{ x^2 \left( \frac{\mathbf{t}_y^2 \mathbf{n}_x^2}{\mathbf{n}^2 \cdot \mathbf{t}^2} - \frac{\mathbf{t}_y^1 \mathbf{n}_x^1}{\mathbf{n}^1 \cdot \mathbf{t}^1} \right) + y^2 \left( \frac{\mathbf{t}_x^1 \mathbf{n}_y^1}{\mathbf{n}^1 \cdot \mathbf{t}^1} - \frac{\mathbf{t}_x^2 \mathbf{n}_y^2}{\mathbf{n}^2 \cdot \mathbf{t}^2} \right) \right. \\
&\quad + xy \left( \frac{(\mathbf{t}_y^2 \mathbf{n}_y^2 - \mathbf{t}_x^2 \mathbf{n}_x^2)}{\mathbf{n}^2 \cdot \mathbf{t}^2} + \frac{(\mathbf{t}_y^1 \mathbf{n}_y^1 - \mathbf{t}_x^1 \mathbf{n}_x^1)}{\mathbf{n}^1 \cdot \mathbf{t}^1} \right) \\
&\quad + x \left( \frac{(\mathbf{c}_y \mathbf{t}_x^2 \mathbf{n}_x^2 - \mathbf{F}^2 \mathbf{n}_x^2)}{\mathbf{n}^2 \cdot \mathbf{t}^2} + \frac{(\mathbf{F}^1 \mathbf{n}_x^1 - \mathbf{c}_y \mathbf{t}_x^1 \mathbf{n}_x^1)}{\mathbf{n}^1 \cdot \mathbf{t}^1} \right) \\
&\quad \left. + y \left( -\frac{(\mathbf{c}_x \mathbf{t}_y^2 \mathbf{n}_y^2 + \mathbf{F}^2 \mathbf{n}_y^2)}{\mathbf{n}^2 \cdot \mathbf{t}^2} + \frac{(\mathbf{F}^1 \mathbf{n}_y^1 + \mathbf{c}_x \mathbf{t}_y^1 \mathbf{n}_y^1)}{\mathbf{n}^1 \cdot \mathbf{t}^1} \right) + \text{constant} \right\}. \tag{12}
\end{aligned}$$

Relationships (10) (11) (12) imply the general formulation

$$V = \frac{1}{2} (C_{x^2} x^2 + C_{y^2} y^2 + C_{xy} xy + C_x x + C_y y + D), \tag{13}$$

for well-chosen coefficients  $C_{x^2}, C_{y^2}, C_{xy}, C_x, C_y$  and  $D$ .

Relationship (13) implies that the function  $V(x, y)$  is piecewise continuously differentiable. Let us denote by  $\nabla V \in \mathbb{R}^2$  the derivatives of  $V$  with respect to the coordinates  $(x, y)$ . The derivatives  $\nabla V$  of the volumes with respect to the coordinates  $(x, y)$  of  $\mathbf{x}^k$  are given by:

$$\nabla V = \frac{1}{2} \begin{pmatrix} 2C_{x^2}x + C_{xy}y + C_x \\ 2C_{y^2}y + C_{xy}x + C_y \end{pmatrix}, \quad (14)$$

and the function  $\nabla V$  is piecewise continuous in the cell, with discontinuities occurring when the intersection point falls in a corner of the cell. Relationships (13) and (14) give explicitly the values of the function  $g$  and its derivatives  $\nabla g$ , and the Newton direction resulting from the resolution of (7).

In the finite volume scheme, the computation of the fluxes through the faces of the cells for the resolution of the flow equations is modified for triple-point configurations in one cell.

The advected volumes located near a face  $f$  can be computed geometrically when the normal vector to the interface, the intersection point between the interface and the cell face (if any) and the coordinates of the vertices of the cell are known. In order to take advantage of the new interface reconstruction, the time step should be chosen such that the advected volumes do not overlap with the triple-point. The modified geometric reconstruction induces different fluxes and can reduce the flotsam of the onion-skin method in multi-phases flows [4, 27], especially for coarse meshes.

## 5. NUMERICAL RESULTS

The tracking of triple-point configurations has been implemented in the three-dimensional code TRUCHAS [12] and numerical experiments are validating our approach. Since TRUCHAS is a three-dimensional code, simulations are reproduced in a thin domain, composed of one layer of one cell along the  $Oz$ -axis to mimic two dimensional situations.

**5.1. Y-shape and T-shape Static Cases.** Static cases are considered to validate the determination of the position of the triple-point. We consider three materials (*e.g.* water, void and graphite) in the square domain  $(-1, 0) \times (-1, 0)$ . For the T-shape configuration, the water and air lie on a planar surface of graphite, with a vertical interface. The triple-point is therefore located exactly in the middle of the domain and there is one adjacent angle that is equal to  $\pi$ . For the Y-shape configuration, the situation is similar except that there is no flat angle adjacent to the triple-point. The domain is split into a finite volume grid of  $3 \times 3 \times 1$  cells. The triple-point is located in the center cell  $(-2/3, -1/3) \times (-2/3, -1/3)$ . For the T-shape configuration, the exact values of the normal vectors to the interface are given respectively by  $\mathbf{n}_{12} = (1, 0)^T$ ,  $\mathbf{n}_{23} = (0, -1)^T$ ,  $\mathbf{n}_{31} = (0, 1)^T$ . The initial guess is placed in a neighborhood of the center of the cell. The tolerance for the stopping criterion of the Newton method is  $\varepsilon = 10^{-13}$ .

Both situations are illustrated in Figure 4 to compare with the actual onion-skin method and show the improvement of the present triple-point method. For the T-shape situation, the first row of Figure 4 shows the reconstruction when the first material is on the upper left, while the second row illustrates the situation when the first material is at the bottom. In the latter case, the ordering of the materials is more appropriate since the horizontal interface is reconstructed more precisely.

As expected, the new reconstruction does not recover the planar interface in the T-shape configuration, but preserves the symmetry. For the Y-shape configuration, the symmetry is also obtained in the central cell. The nature of the method implies

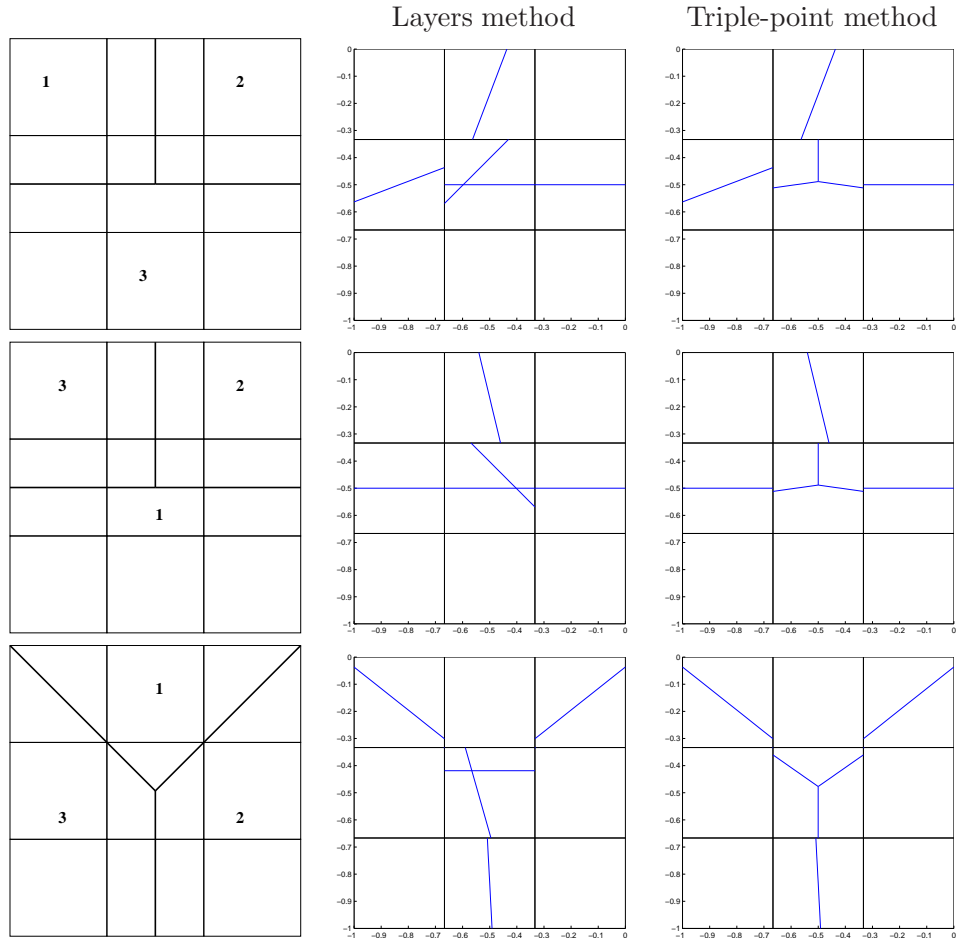


FIGURE 4. Static reconstruction of triple-point configurations. First and second rows: a T-shape situation with different material ordering, third row: a Y-shape situation. The first column is the true setup, the second column shows the reconstruction with the onion-skin model [12, 37] and the third column shows the reconstruction with the triple-point method inside the central cell.

that the results for Y-shape configurations are more accurate than those for the T-shape configurations, for which a sequential PLIC method as in [8] also avoids the crossing of interfaces.

The reconstruction of the interfaces is illustrated in Figure 5 on page 13, for various configurations. The ordering of the materials is given in the left column. These examples allow one to conclude on the robustness of the method in static cases. The Newton method converges approximately in 60 iterations in average, for a tolerance of  $\varepsilon = 10^{-13}$  on the residual  $\|g(x, y)\|$  (without pattern-search initialization) and in less than 20 iterations, for a tolerance of  $\varepsilon = 10^{-6}$  on the residual  $\|g(x, y)\|$ .

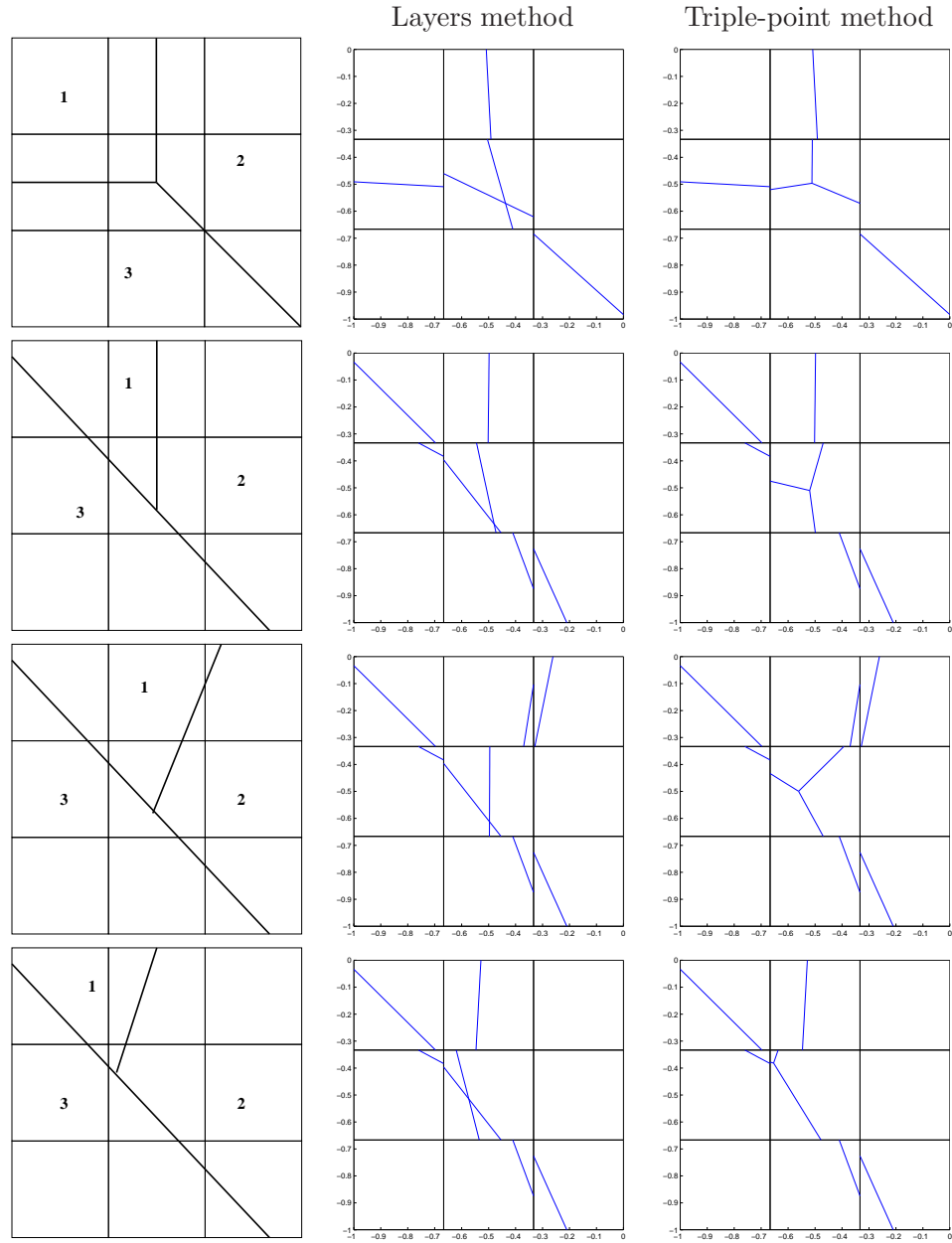


FIGURE 5. Reconstruction of interfaces of various T- and Y-shape configurations: first column: true situation, second column reconstruction with the onion-skin method, third column: reconstruction with the triple-point approach.

**5.2. Translation of a T-shape Configuration.** The T-shape configuration is considered here. The materials are advected with given constant velocity  $v \equiv -1$  along the  $Ox$  axis. Boundary conditions are set accordingly. The order of materials is as follows: material 1 is on the bottom, material 2 on the upper left part and material 3 on the upper right part. The T-shape configuration has to be translated but conserved at each time step. Results are illustrated in Figure 6 and show that the reconstruction of the topology at each time step is improved, in particular for the location of the triple-point.

**5.3. Rotation of a Y-shape Configuration.** The symmetric Y-shape configuration is considered here. The materials are rotated counter-clockwise with constant given velocity  $\mathbf{v} \equiv (-2(x + 0.5), 2(y + 0.5))^T$  around the  $Oz$  axis located in the middle of the two-dimensional domain. The order of materials is as follows: material 1 is on the upper part, material 2 on the right part and material 3 on the left part. The Y-shape configuration is conserved at each time step. Results are illustrated in Figure 7 and show the robustness of the algorithm. The reconstruction of the topology at each time step is improved. Numerical results also show that the direction of the initially vertical interface is consistent with the theoretical value of the rotation angle.

**5.4. Stretching Flows.** We consider the classical "vortex-in-a-box" test case widely treated in the literature, see *e.g.* [2, 29]. The computational domain is the box  $(0, 1) \times (0, 1)$ . The initial liquid domain is a cylinder of radius 0.015 with its center located in  $(0.5, 0.75)$ . It is split in half into two different liquids along the horizontal diameter. The material 1 is on the lower part of the cylinder and the material 2 on the upper part, while the material 3 fills the background domain. The prescribed velocity is given by the stream function:

$$\psi(x, y) = 0.01\pi \sin^2(\pi x/0.1) \sin^2(\pi y/0.1) \cos(\pi t/T_0).$$

This velocity is periodic in time, so that the initial liquid domain is reached again after a time  $T_0$ . Classical values for  $T_0$  in the literature are  $T_0 = 2$  and  $T_0 = 8$ . The dimensions of the domain are  $1 \times 1$ . Various meshes are considered, namely formed by  $16 \times 16$ ,  $32 \times 32$  and  $64 \times 64$  cells. Figure 8 illustrates the interfaces for  $T_0 = 2$  for  $t = 0, 1$  and 2, when the interfaces are reconstructed with the onion-skin algorithm [12, 37]. Figure 9 illustrates the same interfaces for  $T_0 = 2$  for  $t = 0, 1$  and 2, when the triple-point is reconstructed with the method for triple-points presently described. The actual planes reconstructed by the onion-skin and triple-point algorithms in each cell are represented on Figures 8 and 9 respectively, instead of the post-processed level lines of the various materials. Results show that the flotsam is slightly decreased when using the triple-point reconstruction technique for coarser meshes, but the quality of the convergence properties and the robustness of the method when the mesh gets finer are similar.

## 6. CONCLUSIONS

In multiphase flows, the determination of the topology (or geometric configuration) inside cells containing more than two materials is a difficult challenge. A new method for the reconstruction of triple-point interfaces has been presented as an alternative to onion-skin methods. It has been designed to treat any configuration

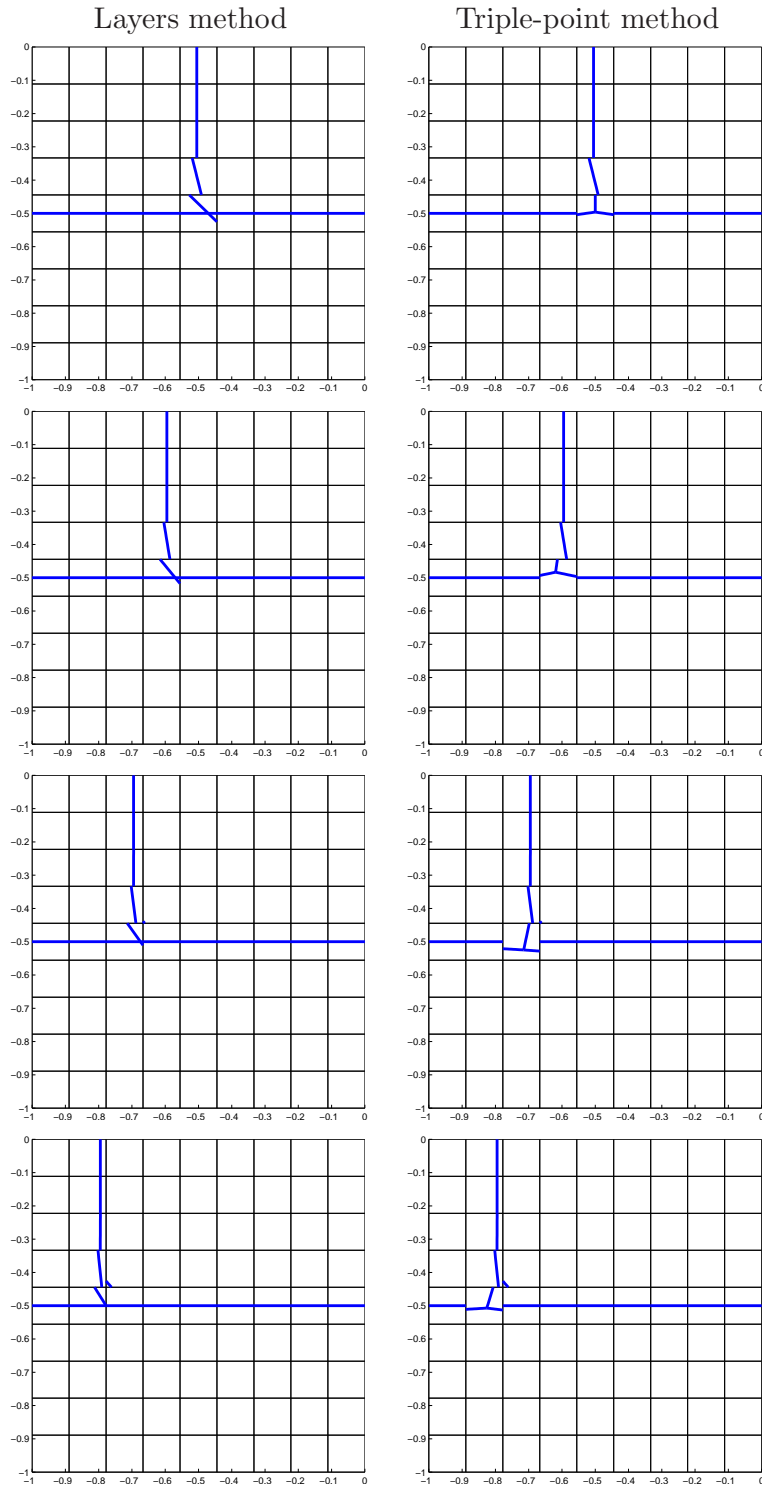


FIGURE 6. Reconstruction of the interfaces for the translation of an orthogonal T-shape configuration at times  $t = 0.001, 0.01, 0.015$  and  $0.020$ . Left: reconstruction with the onion-skin method, right: reconstruction with the triple-point approach.

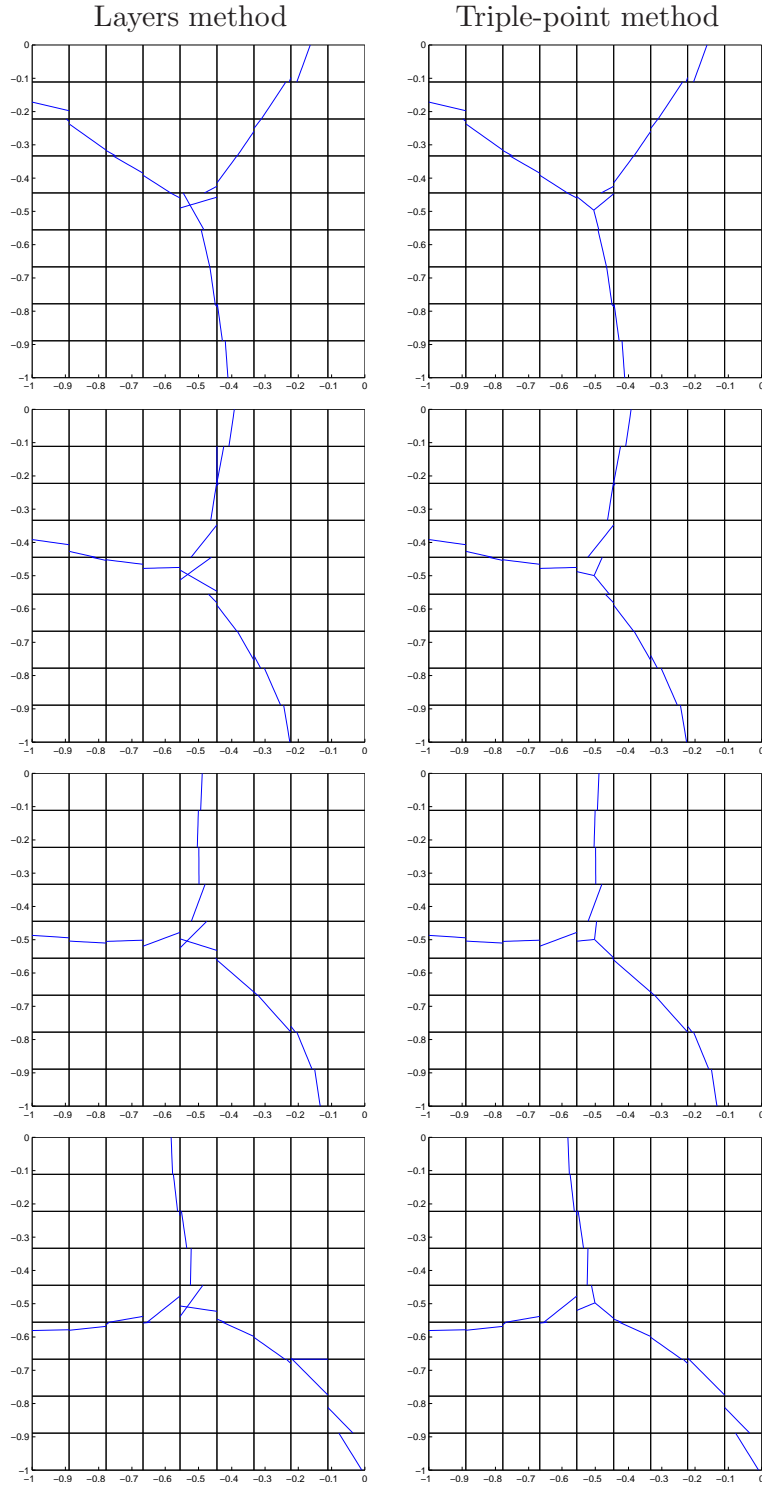


FIGURE 7. Reconstruction of the interfaces for the rotation of a Y-shape configuration at times  $t = 0.01, 0.03, 0.04$  and  $0.05$ . Left: reconstruction with the onion-skin method, right: reconstruction with the present triple-point approach.

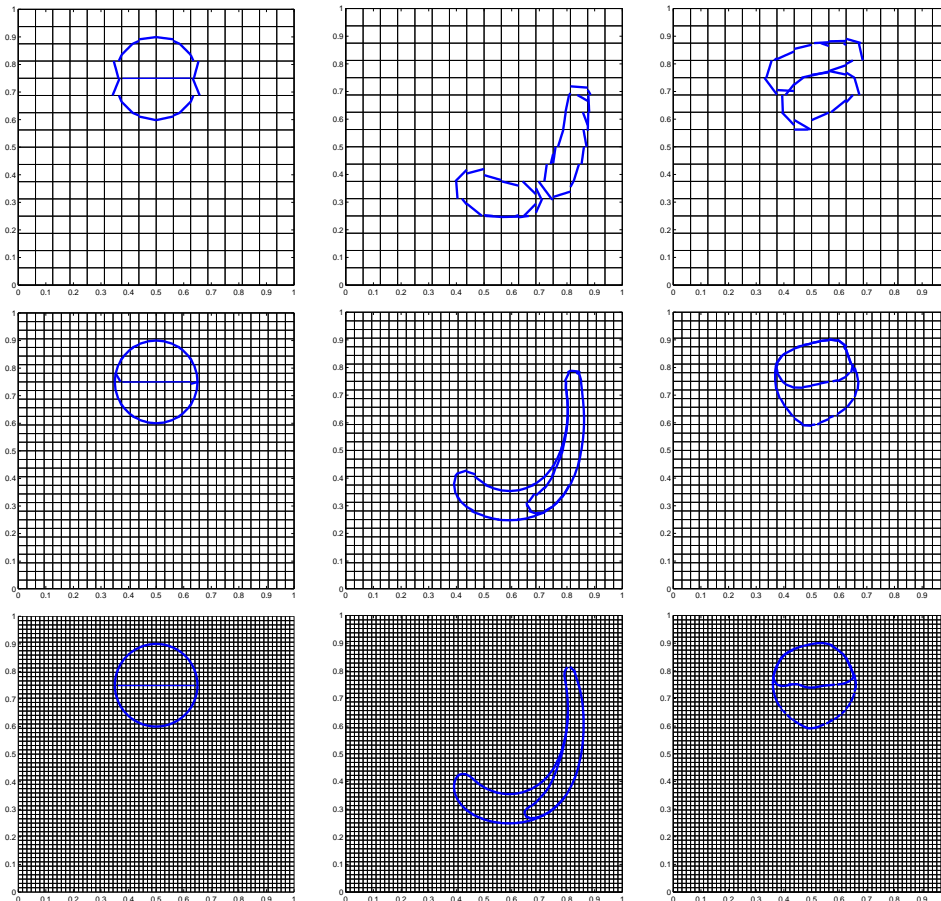


FIGURE 8. Single vortex test case with horizontal interface for  $T = 2$ : solution at times  $t = 0, 1$  and  $2$  (the initial shape is an exact circle with center  $(0.5, 0.75)$ ). Convergence study for decreasing mesh sizes for three materials reconstruction with the onion-skin model [12, 37]. First row: mesh  $16 \times 16 \times 1$  and time step  $0.2$ ; second row: mesh  $32 \times 32 \times 1$  and time step  $0.1$ ; third row: mesh  $64 \times 64 \times 1$  and time step  $0.05$ . Since only the PLIC lines are represented, the interface is on the cell edge if a cell is full or empty.

of three materials in two dimensions, arranged around a triple-point. By construction, this method is more efficient for Y-shaped interfaces than for T-shaped configurations. Numerical results have shown that the proposed method is an efficient alternative to the layers formulation of multi-phases flows, and decreases the flotsam, especially for coarse meshes. The method has proved to be robust in many static and dynamic cases.

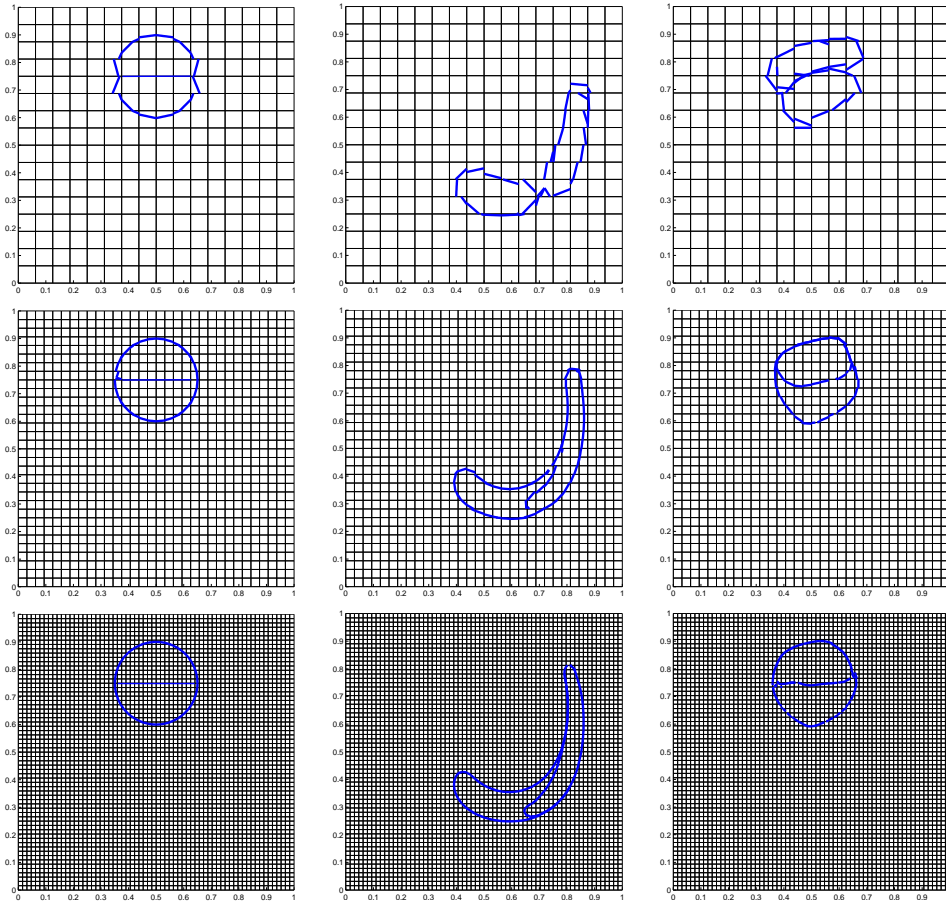


FIGURE 9. Single vortex test case with horizontal interface for  $T = 2$ : solution at times  $t = 0, 1$  and  $2$  (the initial shape is an exact circle with center  $(0.5, 0.75)$ ). Convergence study for decreasing mesh sizes for the three materials reconstruction with the present triple-point algorithm. First row: mesh  $16 \times 16 \times 1$  and time step  $0.2$ ; second row: mesh  $32 \times 32 \times 1$  and time step  $0.1$ ; third row: mesh  $64 \times 64 \times 1$  and time step  $0.05$ . Since only the PLIC lines are represented, the interface is on the cell edge if a cell is full or empty.

#### ACKNOWLEDGMENTS

The Los Alamos National Laboratory and the Telluride project are greatly acknowledged for providing the TRUCHAS software and sponsoring the visits of the first two authors.

#### REFERENCES

- [1] H. T. Ahn and M. Shashkov. Multi-material interface reconstruction on generalized polyhedral meshes. *J. Comput. Phys.*, 226(2):2096–2132, 2007.

- [2] E. Aulisa, S. Manservigi, and R. Scardovelli. A mixed markers and volume-of-fluid method for the reconstruction and advection of interfaces in two-phase and free-boundary flows. *J. Comput. Phys.*, 188:611–639, 2003.
- [3] E. Aulisa, S. Manservigi, and R. Scardovelli. A surface marker algorithm coupled to an area-preserving marker redistribution method for three-dimensional interface tracking. *J. Comput. Phys.*, 197(2):555–584, 2004.
- [4] E. Aulisa, S. Manservigi, R. Scardovelli, and S. Zaleski. A geometrical area-preserving volume-of-fluid advection method. *J. Comput. Phys.*, 192:355–364, 2003.
- [5] F. Aurenhammer. Power diagrams: Properties, algorithms and applications. *SIAM J. Comp.*, 16(1):78–96, 1987.
- [6] A. Caboussat, R. Glowinski, and J. M. Sicilian. Computation of the normal vector to a free surface with a finite element - finite volume mixed method. *C. R. Acad. Sci. Paris, Série I*, 343:431–436, 2006.
- [7] M. H. Cho, Y. C. Lim, and D. F. Farson. Simulation of weld pool dynamics in the stationary pulsed gas metal arc welding process and final weld shape. *Welding Journal*, pages 271–283, 2006.
- [8] B. Y. Choi and M. Bussman. A piecewise linear approach to volume tracking a triple point. *Int. J. Num. Methods Fluids*, 53(6):1005–1018, 2006.
- [9] A. J. Chorin. Flame advection and propagation algorithms. *J. Comput. Phys.*, 35:1–11, 1980.
- [10] R. Codina and O. Soto. A numerical model to track two-fluid interfaces based on a stabilized finite element method and the level set technique. *Int. J. Num. Methods Fluids*, 4:293–301, 2002.
- [11] A. Conn, K. Scheinberg, and Ph. Toint. On the convergence of derivative-free methods for unconstrained optimization. In *Approximation theory and optimization (Cambridge, 1996)*, pages 83–108. Cambridge Univ. Press, Cambridge, 1997.
- [12] E. D. Dendy, J. M. Sicilian, D. B. Kothe, M. Bussmann, M.M. Francois, J. Mohd-Yusof, and S. J. Cummins. Truchas: Physics and algorithms. Technical Report LA-UR-03-0166, Los Alamos National Laboratory, 2003.
- [13] J. E. Dennis and V. Torczon. On the convergence of pattern search algorithms. *SIAM J. Optim.*, 1(4):123–145, 1991.
- [14] V. Dyadechko and M. Shashkov. Moment-of-fluid interface reconstruction. Technical Report LA-UR-05-7571, Los Alamos National Laboratory, 2005.
- [15] V. Dyadechko and M. Shashkov. Reconstruction of multi-material interfaces from moment data. *J. Comput. Phys.*, to appear: , 2008.
- [16] A. V. Fiacco and G. P. McCormick. *Nonlinear Programming: Sequential Unconstrained Minimization Techniques*. John Wiley and Sons, Inc, 1968.
- [17] M. Francois and W. Shyy. Computations of drop dynamics with the immersed boundary method, part 2: Drop impact and heat transfer. *Numerical Heat Transfer Part B*, 44:119–143, 2003.
- [18] M. M. Francois, S. J. Cummins, E. D. Dendy, D. B. Kothe, J. M. Sicilian, and M. W. Williams. A balanced-force algorithm for continuous and sharp interfacial surface tension models within a volume tracking framework. *J. Comput. Phys.*, 213(1):141–173, 2006.
- [19] G. Tryggvason, B. Bunner, A. Esmaeeli, D. Juric, N. Al-Rawahi, W. Tauber, J. Han S. Nas, and Y.-J. Jan. A front tracking method for the computations of multiphase flow. *J. Comput. Phys.*, 169:708–759, 2001.
- [20] C. W. Hirt and B. D. Nichols. Volume of fluid (VOF) method for the dynamics of free boundaries. *J. Comput. Phys.*, 39:201–225, 1981.
- [21] M. Kojima and S. Shindo. Extension of Newton and quasi-Newton methods to systems of PC<sup>1</sup> equations. *Journal of Operations Research Society of Japan*, 29:352–374, 1986.
- [22] D. Kothe, D. Juric, K. Lam, and B. Lally. Numerical recipes for mold filling simulation. In *Proceedings of the Eighth International Conference on Modeling of Casting, Welding, and Advanced Solidification Processes, San Diego, CA*, 1998.
- [23] K. Lipnikov, M. Shashkov, and D. Svyatskiy. The mimetic finite difference discretization of diffusion problem on unstructured polyhedral meshes. *J. Comput. Phys.*, 211:473–491, 2006.
- [24] V. Maronnier, M. Picasso, and J. Rappaz. Numerical simulation of free surface flows. *J. Comput. Phys.*, 155:439–455, 1999.
- [25] J. Nocedal and S. J. Wright. *Numerical Optimization*. Springer-Verlag, 1999.

- [26] W.F. Noh and P. Woodward. *SLIC (Simple Line Interface Calculation)*, volume 59 of *Lectures Notes in Physics*, pages 330–340. Springer-Verlag, 1976.
- [27] J. E. Pilliod and E. G. Puckett. Second-order accurate volume-of-fluid algorithms for tracking material interfaces. *J. Comput. Phys.*, 199:465–502, 2004.
- [28] Y. Renardy and M. Renardy. PROST : A parabolic reconstruction of surface tension for the volume-of-fluid method. *J. Comput. Phys.*, 183:400–421, 2002.
- [29] W.J. Rider and D.B. Kothe. Reconstructing volume tracking. *J. Comput. Phys.*, 141:112–152, 1998.
- [30] R. Scardovelli and S. Zaleski. Direct numerical simulation of free surface and interfacial flows. *Annual Review of Fluid Mechanics*, 31:567–603, 1999.
- [31] S. P. Schofield, R. V. Garimella, M.M. Francois, and R. Loubère. Material order independent interface reconstruction using power diagrams. *Int. J. Num. Methods Fluids*, 56(6):643–659, 2008.
- [32] M. Sussman, K. Smith, M.Y. Hussaini, M. Ohta, and R.-Z. Wei. A sharp interface method for incompressible two-phase flows. *J. Comput. Phys.*, 221(2):469–505, 2007.
- [33] V. Torczon. On the convergence of pattern search algorithms. *SIAM J. Optim.*, 7(1):1–25, 1997.
- [34] R. Trutschel and U. Schellenberger. Dynamic simulation of free surfaces in capillaries with the finite element method. *Int. J. Num. Methods Fluids*, 26:485–495, 1998.
- [35] M. Ulbrich. On a nonsmooth Newton method for nonlinear complementarity problems in function space with applications to optimal control. In M. C. Ferris, O. L. Mangasarian, and J.-S. Pang, editors, *Complementarity: Applications, Algorithms and Extensions*, pages 341–360. Kluwer Academic Publishers, 2001.
- [36] H. Xu and X. W. Chang. Approximate Newton methods for nonsmooth equations. *J. Optim. Theory and Appl.*, 93(2):373–394, 1997.
- [37] D. L. Youngs. Time-dependent multi-material flow with large fluid distortion. In K. W. Morton and M. J. Baines, editors, *Numerical Methods for Fluid Dynamics*, pages 273–285. 1982.

UNIVERSITY OF HOUSTON, DEPARTMENT OF MATHEMATICS, 4800 CALHOUN RD, HOUSTON, TEXAS 77204 - 3008, USA

*E-mail address:* `caboussat@math.uh.edu`

COMPUTER, COMPUTATIONAL AND STATISTICS SCIENCES DIVISION, LOS ALAMOS NATIONAL LABORATORY, LOS ALAMOS, NEW MEXICO 87545, USA

*E-mail address:* `mmfran@lanl.gov`

UNIVERSITY OF HOUSTON, DEPARTMENT OF MATHEMATICS, 4800 CALHOUN RD, HOUSTON, TEXAS 77204 - 3008, USA

*E-mail address:* `roland@math.uh.edu`

NATIONAL CENTER FOR COMPUTATIONAL SCIENCES, OAK RIDGE NATIONAL LABORATORY, OAK RIDGE, TENNESSEE 37831, USA

*E-mail address:* `kothe@ornl.gov`

COMPUTER, COMPUTATIONAL AND STATISTICS SCIENCES DIVISION, LOS ALAMOS NATIONAL LABORATORY, LOS ALAMOS, NEW MEXICO 87545, USA

*E-mail address:* `sicilian@lanl.gov`